



HAL
open science

Computing Geometrical Measures of Topological Holes

Yann-Situ Gazull, Alexandra Bac, Aldo Gonzalez-Lorenzo

► **To cite this version:**

Yann-Situ Gazull, Alexandra Bac, Aldo Gonzalez-Lorenzo. Computing Geometrical Measures of Topological Holes. *Computer-Aided Design*, 2023, 163, pp.103563. 10.1016/j.cad.2023.103563 . hal-04322031

HAL Id: hal-04322031

<https://hal.science/hal-04322031v1>

Submitted on 5 Dec 2023

HAL is a multi-disciplinary open access archive for the deposit and dissemination of scientific research documents, whether they are published or not. The documents may come from teaching and research institutions in France or abroad, or from public or private research centers.

L'archive ouverte pluridisciplinaire **HAL**, est destinée au dépôt et à la diffusion de documents scientifiques de niveau recherche, publiés ou non, émanant des établissements d'enseignement et de recherche français ou étrangers, des laboratoires publics ou privés.

Computing Geometrical Measures of Topological Holes

Yann-Situ Gazull*, Alexandra Bac, Aldo Gonzalez-Lorenzo

Aix Marseille Université, CNRS, LIS, Marseille (France)

Abstract

In algebraic topology, persistent homology is a method that computes the homology of an object growing in time. Intuitively, this technique detects holes and provides information about their importance. By combining this topological approach to a notion of distance, it is possible to define geometric relevant measures associated with these holes. This paper introduces two theoretical methods for computing hole measures in volumetric objects defined by surface meshes. Our approach combines the geometrical and topological properties of the medial axis with the efficiency of persistent homology. We present a practical implementation and results on 3D meshed objects.

Keywords: Geometric Modeling, Algebraic Topology, Medial Axis, Persistent Homology, Surface Mesh.

1. Introduction

In computational geometry, many works aim at analyzing, understanding or classifying geometrical shapes. To carry out this task, they need shape descriptors, which correspond to global or local information of the shape. Topology provides several theoretical descriptors, a large amount of which are highly relevant in the field of computational geometry. Because of its computational properties, homology defines relevant descriptors that provide topological information on the holes of an object.

However, by definition, topology does not take into account geometry. That is why, in order to compute relevant descriptors, a collection of works in computational topology aim at associating geometrical features to topological holes. Such topological/geometric descriptors are useful for classification, as highlighted in [1].

Prior works. In [2], two geometrical measures of topological holes were introduced. The first is the *thickness*, which intuitively represents the “fragility” of a hole and where to break it. The second is the *breadth*, which represents the “size” of a hole and where to fill it. The thickness is visualized as a ball inside the object and the breadth as a ball outside the object.

In the initial paper, those measures were defined and computed in the context of cubical complexes. However cubical complexes are topological structures that inherently integrate a notion of distance and geometry.

The first aim of the present work was to extend the definition for non cubical objects. In addition, our work proposes ideas about how to geometrically measure topological holes, both theoretically and computationally, on volumetric objects. We largely use the notion of medial axis. It is a geometric construction that preserves topological features, and hence is well suited to our problem. We investigate the idea that the computation of the medial axis gives enough information to compute hole measures.

More precisely, instead of performing persistent homology algorithms on the analyzed object (which would require a precise and expensive tetrahedralization), performing these algorithms on the medial axis is sufficient to obtain the thickness and breadth of the holes of the object.

We developed two different approaches. On the one hand, the *link approach* intends to compute every thickness and breadth measures of an object as well as their homological link. On the other hand, the *medial axes approach* is a faster method that computes thickness and breadth measures without their homological link.

The structure of the paper is as follows. In Section 2 we introduce theoretical notions used in following sections such as homology, Alexander duality and medial axis. Section 3 establish a central result concerning the homology of the medial axis. Both of our methods are described in Section 4: we give a definition of hole measures and we then detail the theoretical foundation of both methods. In Section 5 we present results and algorithmic stakes of our approach.

Technical proofs of the lemmas in this paper are provided in the Appendix 6.

2. Theoretical tools

2.1. Homology

Algebraic topology intends to associate algebraic structures to topological objects such that the algebraic properties reflect topological ones. As a branch of this field, homology associates groups to topological objects. Those groups are deeply related to what is intuitively seen as holes. In this section we present a brief introduction to homology and persistent homology. For the sake of simplicity, we focus on the definitions of *simplicial complexes* and $\mathbb{Z}/2\mathbb{Z}$ *simplicial homology*, more general homology definitions can be found in [3].

Definition 2.1 (Simplicial complex). A finite n dimensional *simplicial complex* K is a set of 0-simplices (vertices), 1-simplices (edges), 2-simplices (triangles), 3-simplices (tetrahedra)... n -simplices such that:

*Corresponding author

Email addresses: yann-situ.gazull@univ-amu.fr (Yann-Situ Gazull), alexandra.bac@univ-amu.fr (Alexandra Bac), aldo.gonzalez-lorenzo@univ-amu.fr (Aldo Gonzalez-Lorenzo)

1. for all q -simplex in K , the $(q - 1)$ -simplices of its boundary belong to K .
2. The intersection of two q -simplices is either empty, either a common subspace simplex.

Definition 2.2 (q -chains). Given a n -dimensional complex K , we denote C_q the $\mathbb{Z}/2\mathbb{Z}$ vector space generated by the set of q -dimensional simplices. Elements of C_q are called q -chains.

Definition 2.3 (Chain complex). A *chain complex* (C, ∂) is a sequence of chains together with boundary operators:

$$\cdots \rightarrow C_q \xrightarrow{\partial_q} C_{q-1} \xrightarrow{\partial_{q-1}} \cdots C_1 \xrightarrow{\partial_1} C_0 \xrightarrow{\partial_0} 0$$

with $\partial_q \circ \partial_{q+1} = 0$ (and so $Im(\partial_{q+1}) \subseteq Ker(\partial_q)$).

Definition 2.4 (Homology groups). *Homology groups* of a chain complex (C, ∂) are the following quotients:

$$H_q(C) = Ker(\partial_q) / Im(\partial_{q+1})$$

In our theoretical work, we consider a n -volumetric set $X \subset \mathbb{R}^n$ whose homology groups are finitely generated. Under those conditions, $H_q(X)$ is a $\mathbb{Z}/2\mathbb{Z}$ -vector space of dimension β_q , where β_q is called the q -th *Betti number*. The reduced homology groups are defined as follows:

$$\tilde{H}_0(X) = (\mathbb{Z}/2\mathbb{Z})^{\beta_0-1} \quad \tilde{H}_q(X) = (\mathbb{Z}/2\mathbb{Z})^{\beta_q} \text{ for } q > 0$$

Betti numbers are relevant topological invariants, as they intuitively count the holes of an object in each dimension. For instance, in 3D, β_0 gives the number of connected components (0-holes), β_1 the number of tunnels (1-holes) and β_2 the number of cavities (2-holes). In our theoretical work, we use *singular homology*, which is the counterpart of simplicial homology for arbitrary topological objects.

See [3] for more details on homology and algebraic topology.

Persistent homology. Persistent homology is a recent theory, closely related to Morse theory. It associates a notion of importance to homological holes by following their appearance and disappearance through the growth of a discrete object along time. More precisely, persistent homology captures the changes in homology along a *filtration*.

Definition 2.5 (Filtration). A *filtration* is a sequence $(F_t)_{t \in I}$ of sets verifying $t \leq t' \implies F_t \subset F_{t'}$, where I can be a real interval or a finite ordered set.

Persistence keeps track of the birth and death of holes along the filtration. This information is summed up through a *persistence diagram*:

Definition 2.6 (Persistence diagram). The *persistence diagram* $\mathcal{D}((F_t)_{t \in I})$ of a filtration $(F_t)_{t \in I}$ is a multi set of \mathbb{R}^2 . An element (x, y) of multiplicity $\mu_q^{x,y}$ means that $\mu_q^{x,y}$ holes of dimension q were born in F_x and died entering F_y .

A hole that is still alive at the end of the filtration is represented by a point (x, ∞) . $y - x$ represents the ‘‘lifetime’’ of the hole and significant holes are points of $\mathcal{D}((F_t)_{t \in I})$ lying far from the diagonal $y = x$. See Fig. 4 for an example of persistence diagram.

In practice, X is a finite simplicial complex and the filtration consists in labeling every simplex with its date of birth. The standard algorithm to compute the persistence diagram of a filtration on a simplicial complex X uses operations on the matrix of the boundary operator [4]. It has a complexity in $\mathcal{O}(n^3)$ where n is the number of simplices in X . For more information on persistent homology see [4].

2.2. Alexander Duality

We will write $A \cong B$ iff A and B are homologous (i.e. they have isomorphic homology groups).

Alexander duality provides a link between the homology of an object and its complement in the sphere.

Proposition 2.1 (Alexander Duality). [3, p.255] *If X is a locally contractible nonempty compact of the n -sphere S^n , then:*

$$\forall q, \quad \tilde{H}_q(S^n \setminus X) \approx \tilde{H}^{n-q-1}(X)$$

Where \tilde{H}^q is the q -th reduced cohomology group, and \approx stands for isomorphism.

For instance, Alexander duality implies that we can obtain the Betti numbers of X from those of $S^n \setminus X$ (See an illustration of Alexander duality in Fig. 1).

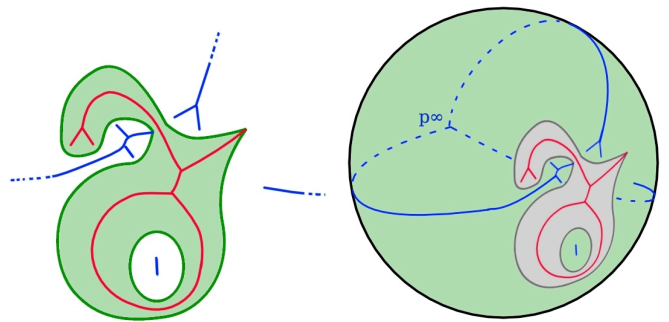


Figure 1: An illustration of Alexander duality and the extended medial axis $M_*(X)$. In green: X (left) and X^c (right). In red: $M_*(X)$. In blue: $\tilde{M}_*(X)$ which equals to $M_*(X^c)$. \mathbb{R}_*^2 is mapped to the sphere S^2 for visual clarity. In 2D, Alexander duality implies that $\beta_0(X) = \beta_1(X^c) + 1$ and $\beta_1(X) = \beta_0(X^c) - 1$: X has one 0-hole and one 1-hole. X^c has two 0-holes but no 1-hole.

Alexander duality is an important tool in our work. It justifies that studying objects in the *Alexandorff extension* of \mathbb{R}^n is more pertinent than in \mathbb{R}^n .

Definition 2.7 (Alexandorff extension [5]). The *Alexandorff extension* of \mathbb{R}^n is $\mathbb{R}_*^n := \mathbb{R}^n \cup \{p_\infty\}$. \mathbb{R}_*^n can be seen as a topological space by considering that the opens of \mathbb{R}_*^n are the opens of \mathbb{R}^n together with all the sets $(\mathbb{R}^n \setminus K) \cup \{p_\infty\}$, where K is a compact of \mathbb{R}^n .

More precisely, we are mapping \mathbb{R}^n to \mathbb{R}_*^n by identifying all the points that are located at infinity to a single point p_∞ . Particularly we can consider that we have $\mathbb{R}^n \subset \mathbb{R}_*^n$.

This construction implies that \mathbb{R}_*^n is homeomorphic to the n -sphere. As a consequence, Alexander duality can be extended to \mathbb{R}_*^n . Moreover, if an object has finitely generated homology groups (for example a finitely triangulable object), its q -homology and q -cohomology groups are isomorphic (see [3, Corollary 3.3]). Therefore, we can deduce the following proposition:

Proposition 2.2 (Alexander Duality extension). *We denote X^c for $\mathbb{R}_*^n \setminus X$. If X is a locally contractible nonempty compact of \mathbb{R}_*^n with finitely generated homology groups, then:*

$$\forall q, \quad \tilde{H}_q(X^c) \approx \tilde{H}_{n-q-1}(X)$$

2.3. Medial axes and Voronoi diagram

The medial axis of a set X is a geometric object that has a large number of characterizations [6]. In this work, we will use the following definitions:

Definition 2.8 (Set of closest boundary points). For any $X \subset \mathbb{R}_*^n$ whose boundary ∂X is nonempty and bounded in \mathbb{R}^n we define:

$$A_X : \mathbb{R}^n \rightarrow \mathcal{P}(\partial X)$$

$$x \mapsto \{s \in \partial X \mid d(x, s) = d(x, \partial X)\}$$

Definition 2.9 (Medial axis). The *medial axis* $\mathcal{M}(X)$ of X is the set of points in \mathbb{R}^n that have two or more closest points on ∂X :

$$\mathcal{M}(X) = \{x \in \mathbb{R}^n \mid |A_X(x)| > 1\}$$

Definition 2.10 (Extended medial axis). The *extended medial axis* $\mathcal{M}_*(X)$ of X is defined as follows:

$$\mathcal{M}_*(X) = \mathcal{M}(X) \cup \{p_\infty\} \subset \mathbb{R}_*^n$$

We define the *inner medial axis* $\check{\mathcal{M}}_*(X)$ and the *outer medial axis* $\hat{\mathcal{M}}_*(X)$ (see Fig. 1 for an illustration) as:

$$\check{\mathcal{M}}_*(X) = \mathcal{M}_*(X) \cap X$$

$$\hat{\mathcal{M}}_*(X) = \mathcal{M}_*(X) \cap X^c = \check{\mathcal{M}}_*(X^c)$$

Voronoi diagram. The medial axis plays an important role in our work. For implementation purpose, a discrete representation of the medial axis is needed. As methods that compute the exact medial axis are too costly in time [7], we focus on approximations of the medial axis. Several algorithms have been developed in the literature, as exposed in [6]. Most of them rely on the notion of *Voronoi diagram* (and its dual the *Delaunay triangulation*) of a sampling of the object's boundary [8, 9, 10] (see Fig. 2).

These approximations are sufficient for our method because, given a precise enough sampling (see section 5.3), they preserve the homology of the medial axis and they provide enough information to capture the important points. Moreover, Voronoi diagrams naturally have a chain complex structure.

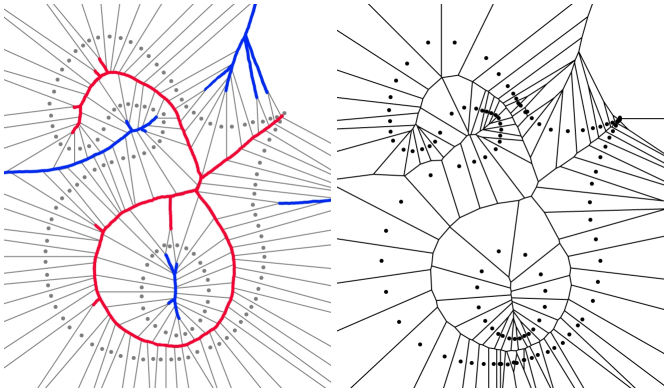


Figure 2: A sampling of the surface and its Voronoi diagram (left). The resulting medial axes approximation is displayed in red and blue. An ϵ -sampling of the surface with its Voronoi diagram (right).

3. Homology Properties of the Medial Axes

In this section we will write $A \equiv B$ iff A is homotopy equivalent to B . In particular $A \equiv B \implies A \cong B$ (see in [3, p.111, Theorem 2.10]).

Our theoretical work strongly relies on the homological properties of the medial axis. More precisely, given an object X , we use the fact that X and its inner medial axis have the same holes. This idea has been studied in the literature, however all theoretical results only apply to bounded objects of \mathbb{R}^n :

Theorem 3.1 (Lieturier [11]). For all open X bounded in \mathbb{R}^n we have $\check{\mathcal{M}}(X) \equiv X$.

For our theoretical work, we require an extension of those properties to unbounded objects in \mathbb{R}_*^n that have a bounded boundary in \mathbb{R}^n . Unfortunately, the proof of Theorem 3.1 can hardly be transposed for unbounded objects.

For now, we achieve to extend homological properties of the medial axis to a specific class of objects that have some ‘‘regularity’’ and can be unbounded (see Theorem 3.3). Hence, we introduce the following definition, which encompasses a large variety of ‘‘real world’’ geometrical shapes:

Definition 3.1 (Regular object). A set $X \subset \mathbb{R}_*^n$ is a *regular object* if it satisfies the following properties:

1. X is a closed set of \mathbb{R}_*^n whose boundary is nonempty bounded in \mathbb{R}^n ;
2. X is a subanalytic set of \mathbb{R}^n (see [12] for a definition of subanalytic sets);
3. $\mathcal{M}_*(X)$ is closed in \mathbb{R}_*^n .

The third required property is the most restrictive assumption because it discards objects with sharp corners. This hypothesis is most probably unnecessary and we are currently working on a proof in this broader context.

We require objects that are subanalytic in order to have the following properties:

Proposition 3.2 (Stability and properties of subanalytic sets). Let X be a subanalytic set of \mathbb{R}^n :

1. The closure \bar{X} , the interior $\overset{\circ}{X}$, the boundary ∂X , the complement $\mathbb{R}^n \setminus X$ and the medial axis $\mathcal{M}(X)$ are subanalytic subsets of \mathbb{R}^n (from theorem 4.1 and 2.1 in [12]);
2. X is triangulable, its homology groups are finitely generated and it is locally contractible (see [13]).

We show the following theorem that states a homological link between an object and its medial axes:

Theorem 3.3 (Medial axes homology). Let X be a regular object of \mathbb{R}_*^n , then

$$\hat{\mathcal{M}}_*(X) \cong X^c \quad \check{\mathcal{M}}_*(X) \cong \overset{\circ}{X}$$

Proof. Given Y a nonempty closed subset of \mathbb{R}_*^n whose boundary ∂Y is bounded in \mathbb{R}^n , we define the following function:

$$p_Y : \hat{\mathcal{M}}_*(Y)^c \longrightarrow Y$$

$$y \longmapsto \underset{x \in Y}{\operatorname{argmin}}(d(x, y))$$

p_Y is well defined and continuous. The proof is technical and can be found in Appendix 6.

Let us X be a *regular object*. Using the function p_X , we can define the following homotopy:

$$\begin{aligned} H : [0, 1] \times \hat{\mathcal{M}}_*(X)^c &\longrightarrow \hat{\mathcal{M}}_*(X)^c \\ (t, y) &\longmapsto tp_X(y) + (1-t)y \end{aligned}$$

- H is well defined because p_X is well defined and for every (t, y) we have $H(t, y) \in \hat{\mathcal{M}}_*(X)^c$.

To prove $H(t, y) \in \hat{\mathcal{M}}_*(X)^c$ for $y \notin X$, consider the maximal closed ball contained in \bar{X}^c centered on y . This ball intersects ∂X only at $p_X(y)$. Having $H(t, y)$ in $\hat{\mathcal{M}}_*(X)$ implies that the ball contains two points of ∂X (more details in Appendix 6).

- H satisfies the properties of a deformation retract from $\hat{\mathcal{M}}_*(X)^c$ to X :

- $X \subset \hat{\mathcal{M}}_*(X)^c$
- $H(0, y) = y$ and $H(1, y) = p_X(y) \in X$
- $\forall t \forall y \in X, H(t, y) = y$
- H is continuous (by continuity of p_X).

As a consequence $\hat{\mathcal{M}}_*(X)^c \equiv X$. This directly implies $\hat{\mathcal{M}}_*(X)^c \cong X$. To conclude the proof, we want to use Alexander duality to “apply” the complementary operator on this homology equivalence. To do that, we need to show that the medial axes satisfies the necessary properties for Proposition 2.2.

- X is a compact subanalytic subset of \mathbb{R}_*^n , so by Theorem 3.2-2, it is a locally contractible nonempty compact with finitely generated homology groups.
- Similarly, we can deduce from Theorem 3.2 that $\hat{\mathcal{M}}_*(X)$ is a locally contractible set of \mathbb{R}_*^n with finitely generated homology groups. In addition, it is compact because it is an intersection of compact sets in \mathbb{R}_*^n : $\check{\mathcal{M}}_*(X) = \mathcal{M}_*(X) \cap X$.

Hence, using Proposition 2.2 on X and $\hat{\mathcal{M}}_*(X)$, we obtain that for all q , $H_q(X^c) \approx H_{n-q-1}(X)$ and $H_q(\hat{\mathcal{M}}_*(X)^c) \approx H_{n-q-1}(\hat{\mathcal{M}}_*(X))$. Therefore the homology equivalence between $\hat{\mathcal{M}}_*(X)^c$ and X translates to: $\hat{\mathcal{M}}_*(X) \cong X^c$. Using Theorem 3.2 we can show that \bar{X}^c is also a *regular object* (see Appendix 6). Applying the whole proof on \bar{X}^c gives: $\hat{\mathcal{M}}_*(X) \cong \check{X}$. \square

All in all, the medial axes characterize the homology of an object and its complement in the Alexandorff extension \mathbb{R}_*^n .

4. Measuring holes in volumetric objects

4.1. Preliminaries

4.1.1. Hole measures definition

Persistent homology can provide geometrical information on topological artifacts if the filtration itself has a geometrical meaning. As stated in the introduction, early works were carried out by Gonzalez-Lorenzo et al. [2] to define and use such a geometric filtration. However, these works heavily relied on the structure of cubical complexes and could not be generalized to more general objects and spaces. In order to overcome those limitations, we first introduce the *signed distance function* and its associated filtration:

Definition 4.1. Given a set X in \mathbb{R}_*^n , the *signed distance function* of X is the following function:

$$\begin{aligned} sdf_X : \mathbb{R}_*^n &\longrightarrow \mathbb{R} \cup \{\pm\infty\} \\ x \in X &\longmapsto -d(x, \partial X) \\ x \in X^c &\longmapsto d(x, \partial X) \end{aligned}$$

Where d is the euclidean distance in \mathbb{R}_*^n (that matches the distance in \mathbb{R}^n and $\forall x, d(p_\infty, x) = \infty$).

Definition 4.2 (*sdf filtration*). We define

$$\mathcal{F}_t(X) := sdf_X^{-1}([-\infty, t])$$

$(\mathcal{F}_t(X))_{t \in \mathbb{R}}$ is a filtration. We refer to it as the *sdf filtration*. It corresponds to erosion if $t < 0$ and dilation otherwise.

The persistence homology of the *sdf filtration* provides different holes, which can be classified in two non-disjoint categories:

- *Early-birth holes*, whose birth date is before 0.
- *Late-death holes*, whose death date is after 0.

Remark. We also use the terms *late-birth* for birth date after 0, and *early-death* for death date before 0.

The holes we are interested in are those in the object at $t = 0$, i.e. those in the intersection of early-birth holes and late-death holes. We refer to them as the *present holes*, they correspond to points in the upper-left quadrant of the persistence diagram (see Fig. 4). Other holes are referred as *non-present holes*.

In this general setting, works of Gonzalez-Lorenzo et al. [2] actually appear as a special case (a discretization) of the *sdf filtration*. Given a present hole with birth date x and death date y , we define the *thickness* T and the *breadth* B of the hole as follows:

$$T = -x \qquad B = y$$

Intuitively, the thickness of the hole corresponds to the fragility of the hole handle. The breadth, on the other side, corresponds to the size of the hole. Those measures can be associated with balls: the *T-ball* (respectively the *B-ball*) is the ball of radius T (respectively B) whose center is the point that induced the birth of the hole at time $-T$ (respectively the death of the hole at time $+B$).

Such points are called *topologically critical points* and play a key role in our work. We refer to *T-balls* and *B-balls* as *hole-balls*.

In the persistence diagram of the *sdf*-filtration, two different informations are provided. On the one hand, the thickness and breadth values, on the other hand their homological relations which state which thickness corresponds to which breadth. We define the notion of *TB-pair* to integrate this subtle topological information. A *TB-pair* is a thickness value together with the breadth value corresponding to the same homological hole. Having only thickness and breadth values without every *TB-pairs* results in what we call a *partial persistence diagram* (see an illustration on Fig. 5).

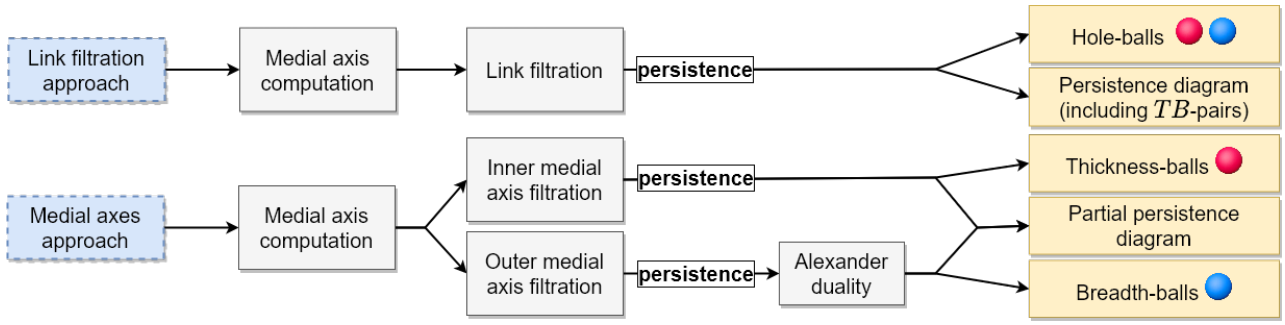


Figure 3: Overview of the two approaches for measuring holes.

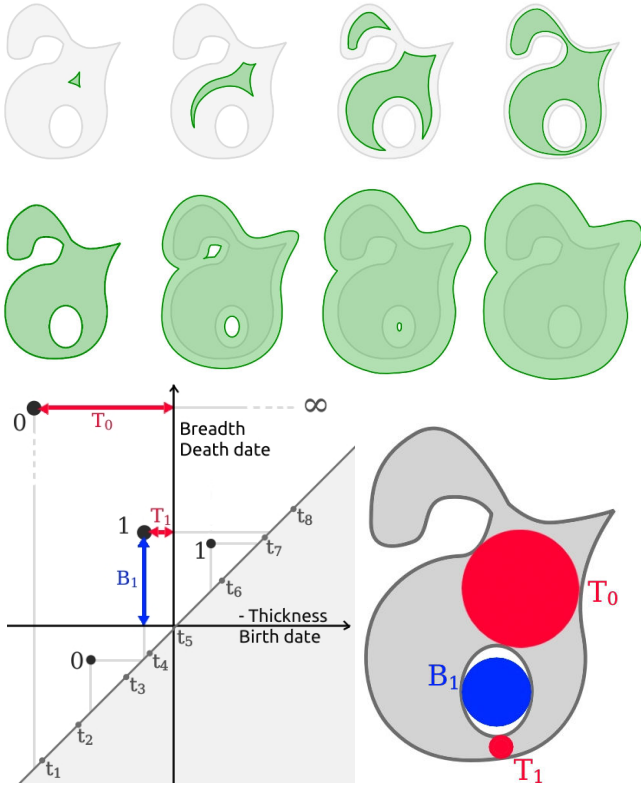


Figure 4: The sdf filtration (in green) of the object X for eight different values: (t_1, \dots, t_8) with $t_5 = 0$.

The persistent diagram is displayed on the bottom left: X has a 0-hole (born at before t_1 that does not die) and a 1-hole. Their respective balls are represented on the right (breadth in blue, thickness in red).

The persistence diagram shows that two non-present holes appeared during the filtration, a 0-hole with lifetime within $[t_2, t_4]$ and a 1-hole with lifetime within $[t_5, t_7]$.

4.1.2. Overview of our approach

The aim of our work is to study the properties of such hole measures and provide algorithms to compute them for 3D shapes. Computationally, we are dealing with 3D compact volumes, the boundary of which is an oriented mesh (2-manifold). Yet, our theoretical work is more general and applies to \mathbb{R}^n .

We aim at computing the persistence diagram of the sdf filtration and the topologically critical points associated to each hole because it provides the hole-balls. A naive and costly idea would be to triangulate \mathbb{R}^3 in order to approximate the dilation and erosion of the object. Nevertheless, our work shows that computing the persistence on a filtration built using the medial axis of our object is sufficient to obtain hole measures.

We develop two approaches. The first one is the *link approach* and is developed in Section 4.2. It consists in building a single filtration that links the inner and outer medial axes along the sdf values. Computing the persistence of this filtration gives every hole-ball. In addition, it gives the complete persistence diagram of the sdf filtration which provides the TB -pairs.

The second approach is the *medial axes approach* and is developed in Section 4.3. It consists in building two distinct filtrations: one based on the sdf filtration restricted to the inner medial axis, the other based on the opposite sdf filtration restricted to the outer medial axis.

We show that every T -ball can be obtained from the persistence of the inner medial axis filtration and every B -ball can be deduced from the persistence of the outer medial axis filtration using Alexander duality.

In practice, this approach is faster because the total size of the inner and outer medial axis filtration is much smaller than the size of the filtration used in the link approach. However, it only computes a partial persistence diagram and does not provide the TB -pairs. This might not be a problem, as the user might only be interested in the balls and not in their homological relations.

Both approaches are summarized in Fig. 3.

4.2. Link approach

In the sdf filtration, it appears that the interesting homological information are localized on specific locations in space-time: the topologically critical points and their associated birth and death dates. Therefore, the whole sdf filtration is not necessary and we can focus on smaller sets. As the medial axis preserves homology and topologically critical points (see Section 4.3), it appears as a good candidate to build a simpler filtration.

The link approach was developed with the idea of reducing the sdf filtration to its crucial part. It consists in a single filtration that links the inner medial axis to the outer one along the sdf values.

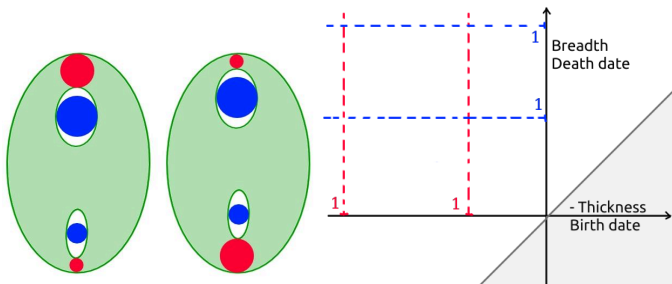


Figure 5: Two objects (left) that have the same partial persistence diagram (right). They have different TB -pairs: in the first shape, the big B -ball is associated with the big T -ball whereas it is not the case in the second one.

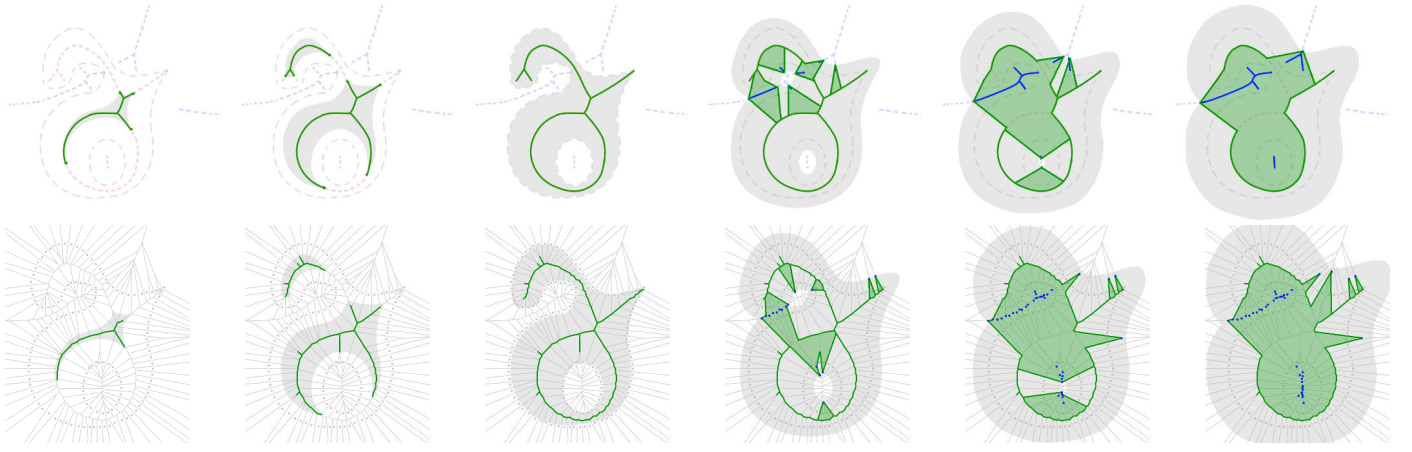


Figure 6: The link filtration (above) and its discrete counterpart the Voronoi filtration (below).

Definition 4.3 (Link Graph). We define the bipartite *link graph* $G_X(V, E)$ of X with:

$$\begin{aligned} V &:= \mathcal{M}_*(X) = \check{\mathcal{M}}_*(X) \cup \hat{\mathcal{M}}_*(X) \\ E &:= \{(\check{c}, \hat{c}) \in \check{\mathcal{M}}_*(X) \times \hat{\mathcal{M}}_*(X) / A_X(\check{c}) \cap A_X(\hat{c}) \neq \emptyset\} \end{aligned}$$

We define the link function:

$$\begin{aligned} \xi : \mathcal{P}(V) &\rightarrow \mathcal{P}(\mathbb{R}_*^n) \\ C &\mapsto C \cup \bigcup_{(\check{c}, \hat{c}) \in E \cap C^2} \text{conv}(\check{c}, \hat{c}) \end{aligned}$$

Definition 4.4 (Link filtration). We define

$$\xi_t(X) := \xi(\mathcal{F}_t(X) \cap \mathcal{M}_*(X))$$

$(\xi_t(X))_{t \in \mathbb{R}}$ is a filtration. We refer to it as the *link filtration* (see Fig. 6).

We conjecture that the link filtration provides the same persistence diagram as the *sdf* filtration. Moreover, we also think it provides the same topologically critical points.

Conjecture 4.1 (Link filtration persistence).

$$\mathcal{D}((\mathcal{F}_t(X))_{t \in \mathbb{R}}) = \mathcal{D}((\xi_t(X))_{t \in \mathbb{R}})$$

In addition, the topologically critical points of $(\mathcal{F}_t(X))_{t \in \mathbb{R}}$ are exactly the topologically critical points of $(\xi_t(X))_{t \in \mathbb{R}}$.

For $t < 0$ the link filtration corresponds to what we call the inner medial axis filtration $(\mathcal{F}_t(X) \cap \mathcal{M}_*(X))_{t < 0}$. We have proved the part of the conjecture where $t < 0$ using the geometrical and topological properties of the inner medial axis (see Theorem 4.4 and Theorem 4.5 in Section 4.3). The conjecture is under work for $t > 0$, where the link filtration links the inner medial axis to the outer one. Fortunately, experiments tend to validate the conjecture as pointed out in Section 5.

The main advantage of this filtration is that it can be approached algorithmically using a Voronoi diagram (see Fig. 6). Indeed, the Voronoi diagram of a surface sampling also provides an approximation of the link function. More precisely, the duals of Delaunay faces that lie on ∂X give an approximation of ξ . We define the *Voronoi filtration*, which can be seen as a discrete version of the link filtration:

Definition 4.5 (Voronoi Filtration). Consider the nD Voronoi diagram of a sampling on ∂X .

We build a filtration by labelling each Voronoi cell to a value: the value of a Voronoi vertex is its *sdf* value. The value of a given i -cell c is defined as the maximum between the values of the $(i - 1)$ -cells in the boundary of c . The induced filtration is the *Voronoi filtration* and is the discrete counterpart of the link filtration. See an illustration in Fig. 6.

4.3. Medial axes approach

Besides being essential for the computation of the *TB*-pairs, the link between the two medial axes is not necessary to obtain the hole-balls. Moreover, this link is quite expensive when dealing with the Voronoi filtration in practice. This motivated the medial axes approach, in which we discard the link and build two distinct filtrations: the *inner medial axis filtration* and *outer medial axis filtration* which respectively give every *T*-ball and *B*-ball, without the *TB*-pairs.

4.3.1. Obtaining thickness balls from the inner medial axis

In this part, a deeper link between the topology and the geometry of $\check{\mathcal{M}}_*(X)$ and X is introduced: the persistence diagram of the *sdf* filtration on $] - \infty, 0]$ is the same as the one obtained with the *sdf* filtration restricted to $\check{\mathcal{M}}_*(X)$.

This result is stated in Theorem 4.4. It implies that computing the persistent homology of $\check{\mathcal{M}}_*(X)$ on $] - \infty, 0]$ provides early-birth and early-death dates with their associated topologically critical points and therefore the *T*-balls of X .

Definition 4.6 (Inner medial axis filtration). Given t , we define $\check{\mathcal{M}}_t(X) := \mathcal{F}_t(X) \cap \check{\mathcal{M}}_*(X)$. The sequence $(\check{\mathcal{M}}_t(X))_{t \in] - \infty, 0]}$ is a filtration. We refer to it as the *inner medial axis filtration*. Note that this definition is similar to the definition of the λ -medial axis [14].

Theorem 4.2. Given X a regular object and a filtration value $t < 0$ such that $\mathcal{F}_t(X)$ is nonempty:

$$\check{\mathcal{M}}_*(\mathcal{F}_t(X)) = \check{\mathcal{M}}_t(X)$$

Let $t < 0$. For simplicity we will write \mathcal{F}_t instead of $\mathcal{F}_t(X)$. The proof of Theorem 4.2 requires the two following properties:

Lemma 4.2.1. 1. $\partial \mathcal{F}_t \subset \text{sdf}_X^{-1}(\{t\})$

$$2. \forall c \in \mathcal{F}_t, \quad d(c, \partial X) = d(c, \partial \mathcal{F}_t) - t$$

The proof of this lemma is technical and can be found in Appendix 6.

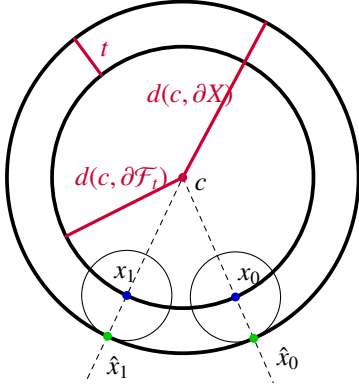


Figure 7: Illustration of the different points defined in the proof of the Theorem 4.2.

Proof of Theorem 4.2.

Proof of $\check{M}_t(X) \subset \check{M}(\mathcal{F}_t)$. Let $c \in \check{M}_t(X)$. We have $c \in \check{M}(X)$ so we choose $\hat{x}_0, \hat{x}_1 \in A_X(c)$ such that $\hat{x}_0 \neq \hat{x}_1$. As $d(c, \partial X) > -t > 0$, we define:

$$x_0 = \mu c + (1 - \mu)\hat{x}_0 \quad x_1 = \mu c + (1 - \mu)\hat{x}_1$$

with $\mu = \frac{-t}{d(c, \partial X)} \in]0, 1[$. We hence have $x_0 \neq x_1$. To prove $c \in \check{M}(\mathcal{F}_t)$, let us show that x_0 and x_1 belong to $A_{\mathcal{F}_t}(c)$. Let $i \in \{0, 1\}$. As $c \in \mathcal{F}_t$, we only need to show $d(x_i, c) = d(c, \partial \mathcal{F}_t)$ and $x_i \notin \mathcal{F}_t$:

$$\begin{aligned} d(x_i, c) &= (1 - \mu)d(c, \hat{x}_i) = \frac{d(c, \partial X) + t}{d(c, \partial X)} d(c, \partial X) \\ &= d(c, \partial \mathcal{F}_t) \quad \text{by Lemma 4.2.1-2} \end{aligned}$$

Moreover, we have:

$$d(x_i, \hat{x}_i) = \mu d(c, \hat{x}_i) = -t$$

So, as $\hat{x}_i \in \partial X$, $d(x_i, \partial X) \leq -t$. This implies $x_i \notin \mathcal{F}_t$.

Proof of $\check{M}(\mathcal{F}_t) \subset \check{M}_t(X)$. Let $c \in \check{M}(\mathcal{F}_t)$. We choose $x_0, x_1 \in A_{\mathcal{F}_t}(c)$ such that $x_0 \neq x_1$.

Let $i \in \{0, 1\}$. Let $\hat{x}_i \in A_X(x_i)$. $x_i \in \partial \mathcal{F}_t$ so by Lemma 4.2.1-1 we have $d(\hat{x}_i, x_i) = -t$. By triangle inequality we have:

$$\begin{aligned} d(\hat{x}_i, c) &\leq d(\hat{x}_i, x_i) + d(x_i, c) \leq -t + d(c, \partial \mathcal{F}_t) \\ &\leq d(c, \partial X) \quad \text{by Lemma 4.2.1-2} \end{aligned}$$

As \hat{x}_i is in ∂X we obtain $d(c, \partial X) = d(\hat{x}_i, c)$ so \hat{x}_i belongs to $A_X(c)$. To conclude the proof, let us show that $\hat{x}_0 \neq \hat{x}_1$: the previous triangle inequality resulted in an equality, which means that \hat{x}_i, x_i and c are co-linear. As $d(c, \partial X) > -t > 0$, we get:

$$x_0 = \mu c + (1 - \mu)\hat{x}_0 \quad x_1 = \mu c + (1 - \mu)\hat{x}_1$$

with $\mu = \frac{-t}{d(c, \partial X)} \in]0, 1[$. Hence we have $\hat{x}_0 \neq \hat{x}_1$ since $x_0 \neq x_1$. \square

Theorem 4.2 implies the following property:

Corollary 4.3. *Given X a regular object and $t \leq 0$ such that $\mathcal{F}_t(X) \neq \emptyset$:*

$$\mathcal{F}_t(X) \cong \check{M}_t(X)$$

Proof. $\overline{\mathcal{F}_t(X)}$ is a regular object. Indeed, it is closed with nonempty bounded boundary, subanalytic (see [14]) and its medial axis is closed (by Theorem 4.2).

Theorem 3.3 on $\overline{\mathcal{F}_t(X)}$ gives:

$$\check{M}_*(\mathcal{F}_t(X)) \cong \mathcal{F}_t(X)$$

Combined to Theorem 4.2 we get the wanted result. \square

As a consequence, the *sdf* filtration persistence diagram of X on $] - \infty, 0]$ can be obtained by performing the persistence algorithm on its inner medial axis.

Theorem 4.4 (Hole measures from inner medial axis). *Given X a regular object of \mathbb{R}_*^d :*

$$\mathcal{D}((\mathcal{F}_t(X))_{t \in] - \infty, 0]}) = \mathcal{D}((\check{M}_t(X))_{t \in] - \infty, 0]})$$

The studied interval is $] - \infty, 0]$, so this diagram gives every early-birth and early-death date, but we also need the ball centers in order to fully obtain the T -balls. Fortunately, we have the following proposition, which can be deduced from results in [15, 16]:

Proposition 4.5. *The topologically critical points of $(\mathcal{F}_t(X))_{t \in] - \infty, 0]}$ are exactly the topologically critical points of $(\check{M}_t(X))_{t \in] - \infty, 0]}$.*

As the standard persistence algorithm also computes the topologically critical points, performing the persistence algorithm on $(\check{M}_t(X))_{t \in] - \infty, 0]}$ fully provides the T -balls.

4.3.2. Obtaining breadth balls from the outer medial axis

In this part we aim at capturing the persistence on $[0, +\infty[$ (i.e. the B -balls, late-death and late-birth dates) using the outer medial axis and Alexander duality. To begin with, given our regular object X , we define the filtration of the complement:

Definition 4.7 (*sdf^c* filtration). $(\mathcal{F}_t(X^c))_{t \in \mathbb{R}}$ is a filtration. We refer to it as the *sdf^c* filtration (see Fig.8). Intuitively, erosions in the *sdf* filtration correspond to dilations in the *sdf^c* filtration and vice-versa.

The persistence diagram of the *sdf* filtration of X on $[0, +\infty[$ can be deduced from the diagram of the *sdf^c*-filtration restricted to $\hat{M}_*(X)$. This result is stated more precisely in Corollary 4.8.

Corollary. 4.3 applied to $\overline{X^c}$ gives:

Corollary 4.6. *Given X a regular object and $t \leq 0$ such that $\mathcal{F}_t(X^c) \neq \emptyset$:*

$$\mathcal{F}_t(X^c) \cong \check{M}_t(X^c)$$

As in section 4.3.1, this implies that the persistence diagram of X^c on $] - \infty, 0]$ can be obtained by computing the persistence diagram of the outer medial axis of X . Then we need to use Alexander duality to deduce the persistence diagram of X on $[0, +\infty[$. This deduction is stated in the following conjecture, which is still under work:

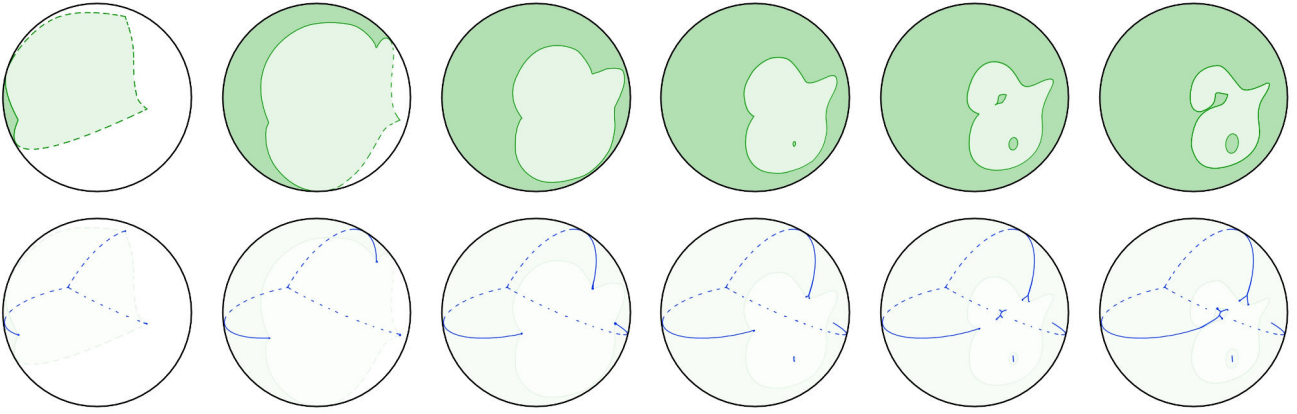


Figure 8: The sdf^c filtration in \mathbb{R}_*^2 : $(\mathcal{F}_t(X^c))_{t \in [-\infty, 0]}$ (above). The filtration of the outer medial axis in \mathbb{R}_*^2 : $(\check{\mathcal{M}}_t(X^c))_{t \in [-\infty, 0]}$ (below). \mathbb{R}_*^2 is displayed as the 2-sphere.

Conjecture 4.7 (Alexander persistence duality). *Considering two filtrations $(F_t)_{t \in I}$ and $(F'_t)_{t \in I}$ such that $\forall t \in I, (F_t)^c = F'_{-t}$, we have:*

$$\mathcal{D}((F_t)_{t \in I}) = \mathcal{D}^c((F'_t)_{t \in I})$$

Where $\mathcal{D}^c(\cdot)$ stands for the dual of the underlying persistence diagram following Alexander duality: the i -holes of coordinates (x, y) become $(n - i - 1)$ -holes of coordinates $(-y, -x)$ (with a special case for 0-dimensional holes).

Corollary 4.6 and Conjecture 4.7 imply the following corollary:

Corollary 4.8 (Hole measures from outer medial axis). *Assuming Conjecture 4.7:*

$$\mathcal{D}((\mathcal{F}_t(X))_{t \in [0, +\infty[}) = \mathcal{D}^c((\check{\mathcal{M}}_t(X^c))_{t \in [-\infty, 0]})$$

In particular, computing the persistent homology on $\hat{\mathcal{M}}_*(X)$ with the sdf^c -filtration provides every late-death and late-birth dates of X .

To fully find the B -balls of X , we also need a proposition analogous to Proposition 4.5 which can be deduced from results in [15, 16] combined with Conjecture 4.7:

Corollary 4.9. *Assuming Conjecture 4.7, the topologically critical points of $(\mathcal{F}_t(X))_{t \in [0, +\infty[}$ are exactly the topologically critical points of $(\check{\mathcal{M}}_t(X^c))_{t \in [-\infty, 0]}$, but they appear in the reverse order.*

Hence, the persistence diagram of the outer medial axis $\hat{\mathcal{M}}_*(X)$ with the sdf^c -filtration induces the deduction of every late-death and late-birth date of X with their critical points. Therefore, it fully provides the B -balls.

All in all, computing the persistence of the inner and outer medial axes of X (using their appropriate filtration) gives enough information to obtain every hole-ball of X .

5. Implementation and validation on 3D objects

5.1. Implementation and results

We implemented the two methods for 3D models in C++ using *CGAL* [17] for geometry and *PHAT* [18] for persistent homology. We experimented our methods on different 3D models, mostly from the Thingi10k [19] dataset. We focused on

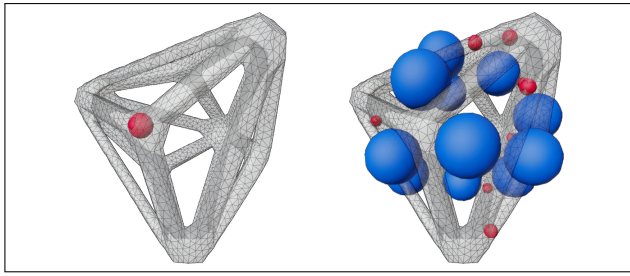
objects that we regarded as topologically interesting (non trivial shapes with multiple holes of different dimensions) and we used uniform samplings with different densities to build the medial axis approximation using Voronoi diagram. The code can be found on a GitHub repository [20].

Given a correct approximation of the medial axis, the results obtained using the medial axes approach are valid. We tested the method on tricky objects such as the *knot* (Fig. 9d), which seems complicated but has only one 1-dimensional hole. We also tested the method on *egg-in-a-box* (Fig. 9b), which consists in a component within another component. The algorithm returned the appropriate 0-dimensional hole-balls corresponding to the two components and the 2-dimensional hole-balls corresponding to the inside of the box. We tested the approach on symmetrical objects such as the *hollow-cubic-ball* (Fig. 9c) and the *triakis-tetrahedron* (Fig. 9a). As expected, the algorithm returned 1-dimensional T -balls (respectively B -balls) with almost exactly the same radii.

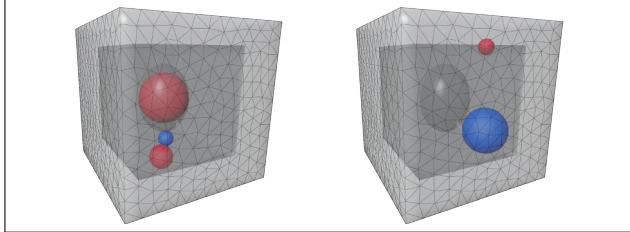
Given the same approximation of the medial axis, the Voronoi filtration gives similar results as the medial axes approach: nearly the same thickness and breadth values and most of the time close ball centers. In addition, the Voronoi filtration provided the expected TB -pairs. For instance, in the *four-components* object (Fig. 9e), each 0-dimensional T -ball inside a component is related to the 0-dimensional B -ball that links this component to the others. Similarly, the 1-dimensional T -ball of a holey component is related to the 1-dimensional B -ball in the same component. In the *eight* object (Fig. 9f), each 1-dimensional T -ball is related to its tangent B -ball.

All in all, this provides an experimental validation of the Link approach, which is not theoretically established yet (see Conjecture 4.1).

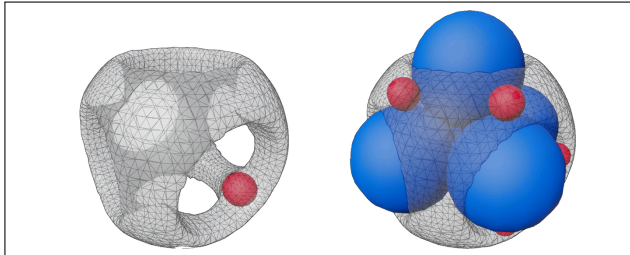
Notice that in some cases, the ball centers returned by the two methods are far apart. This is due to the unstability of topologically critical points which might not be unique, for instance on long portions with a constant distance to medial axes (as between the rings in Fig. 10a 10b).



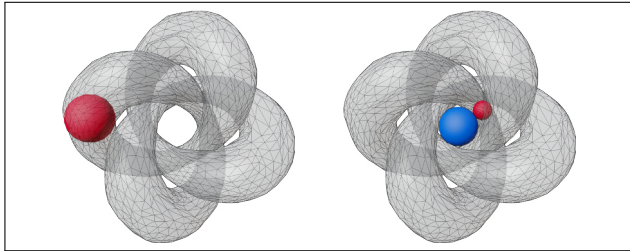
(a) 0-dimensional (left) and 1-dimensional (right) hole-balls of *triakis-tetrahedron*.



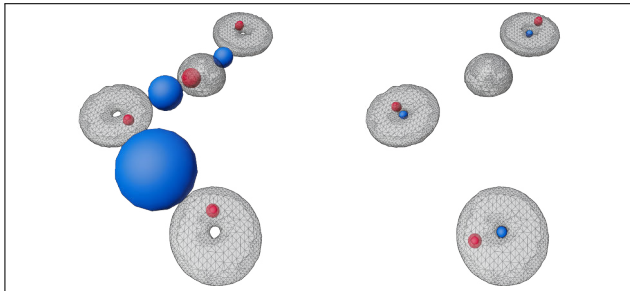
(b) 0-dimensional (left) and 2-dimensional (right) hole-balls of *egg-in-a-box*.



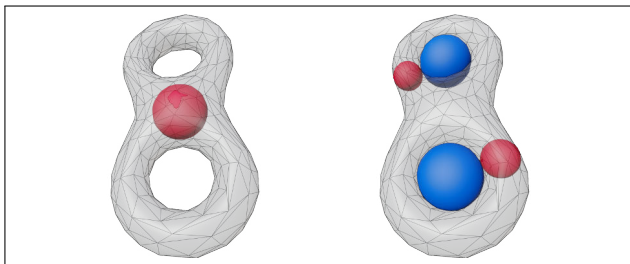
(c) 0-dimensional (left) and 1-dimensional (right) hole-balls of a *hollow-cubic-ball*.



(d) 0-dimensional (left) and 1-dimensional (right) hole-balls of *knot*.

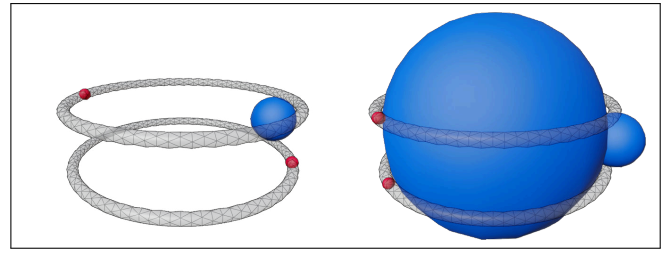


(e) 0-dimensional (left) and 1-dimensional (right) hole-balls of *four-components* with three 1-holes.

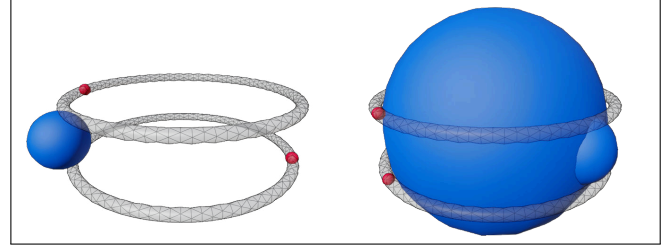


(f) 0-dimensional (left) and 1-dimensional (right) hole-balls of *eight*.

Figure 9



(a) 0-dimensional (left) and 1-dimensional (right) hole-balls of *two-rings* using **medial axes approach**.



(b) 0-dimensional (left) and 1-dimensional (right) hole-balls of *two-rings* using **link approach**.

Figure 10: Comparison between the hole-balls computed by both approaches.

5.2. Catching the right ball centers

Using both methods with filtration defined by the *sdf* values at Voronoi vertices can result in balls not exactly located where they are expected. This is due to the fact that in rare cases, some topologically critical points are not approached by Voronoi vertices, even though they belong to the induced medial axis approximation and whatever the precision of the initial sampling is (see Fig. 11c).

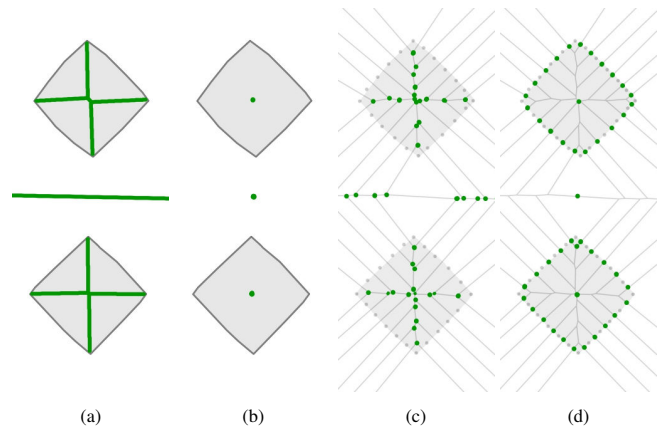


Figure 11: Two squares and its medial axis in green (a), its topologically critical points (b), the Voronoi vertices of a surface sampling (c) and the Delaunay critical points of this sampling (d).

The Voronoi vertices miss the central topologically critical point (c) whereas the Delaunay critical points catch all of them (d).

Inspired by [9, 15, 16], we define a new notion of “critical points”:

Definition 5.1 (Delaunay critical points). Given a Delaunay triangulation of a point set P , a *Delaunay critical point* is the intersection point of a Delaunay face with its dual Voronoi face (if the intersection exists). These critical points actually correspond to topologically critical points of the discrete object P .

Despite the fact that topologically critical points are not approached by Voronoi vertices in some particular cases, we con-

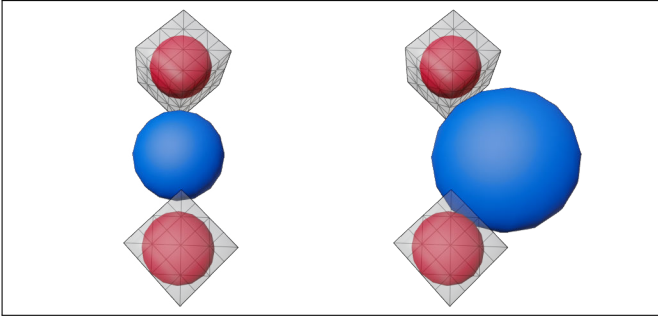


Figure 12: *two-cubes* object and its 0-dimensional hole-balls obtained with (left) and without (right) taking into account Delaunay critical points.

jecture that under some regularity assumptions they can always be approached by Delaunay critical points (see Fig. 11):

Conjecture 5.1. *Given a set A we denote $T(A)$ the set of topologically critical points induced by A .*

Let X be a regular object of \mathbb{R}_^n . Suppose that for all ϵ , P_ϵ is an ϵ -sampling of ∂X . Then we have:*

$$\max_{c \in T(X)} d(c, T(P_\epsilon)) \xrightarrow{\epsilon \rightarrow 0} 0$$

We implemented an improvement of our methods that incorporates Delaunay critical points within the filtrations. To realize this task, we only modify the *sdf* values of some cells and associate each critical cell to its Delaunay critical point. As computing intersections between Delaunay and Voronoi cells is cheap, the extra cost is negligible. This improvement has been tested experimentally without any wrong results (see Fig. 12).

Conjecture 5.1 would theoretically guarantee that our implemented methods indeed approximate the hole measures, as increasing the sampling precision would make the balls converge to the true hole-balls.

5.3. Heuristics for sampling

The major limitation of our approach is the quality of the sampling: in order to obtain the theoretical guarantees on homology that imply the correctness of our methods, we need a sampling accurate enough. More precisely, the perfectly suited sampling would be an ϵ -sampling, which is a sampling with a density varying according to the distance to the medial axes (see Fig. 2):

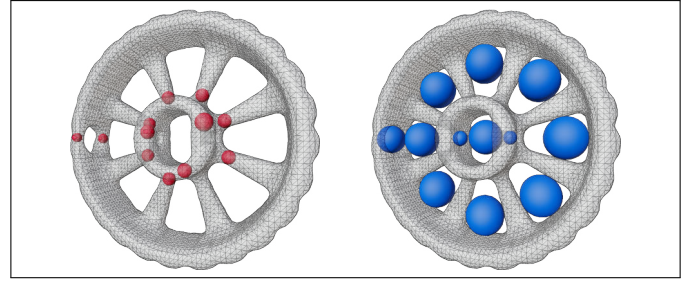
Definition 5.2 (ϵ -sampling [9]). An ϵ -sampling of the surface ∂X of X is a set $P \subset \partial X$ such that:

$$\forall x \in \partial X, \exists p \in P / d(x, p) \leq \epsilon \cdot d(x, \mathcal{M}_*(X))$$

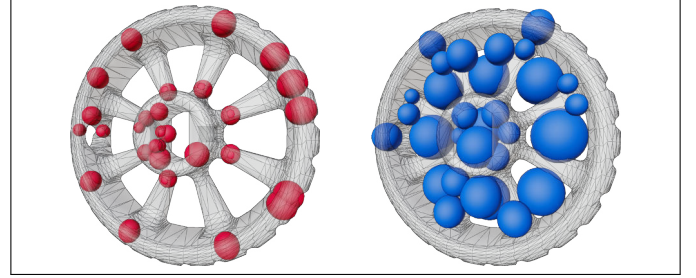
It has been showed in [9, 8] that an ϵ -sampling with ϵ small enough provides topological guarantees. The sampling is important in practice because a sampling not dense enough results in wrong holes (see Fig. 13a and Fig. 13b), whereas an overly dense one could be too costly because it creates a significant number of faces.

5.4. Complexity

The complexity of the algorithm highly depends on the initial sampling for computing the Voronoi approximation: the complexity of the persistence algorithm is $O(m^3)$ where m is the number of cells in the filtration (see [4]). In our methods m is bounded by the size of the Voronoi approximation of the medial axis. Fortunately, if the sampling of size n is uniform enough, it is known



(a) 1-dimensional T -balls (left), 1-dimensional B -balls (right) of a gear obtained from an appropriate sampling.



(b) 1-dimensional T -balls (left), 1-dimensional B -balls (right) of a gear obtained from a bad sampling.

Figure 13

that the computation and the size of the Voronoi diagram is linear in n (see [21, 22]). This implies that the theoretical complexity in time of our two methods is $O(n^3)$.

Fortunately, with a sparse matrix implementation, the persistence algorithm takes less time in practice: as pointed out in [4] the running time is at most proportional to the sum of squares of hole lifetimes.

This gives a total complexity of $O(\beta n^2)$ where β is the number of holes and n the number of samples.

It is worth noting that the medial axes approach is theoretically faster. Indeed, the Voronoi filtration has a lot more cells than medial axes filtrations combined (about the number of Delaunay cells that belong to the object boundary). This is the counterpart of only computing a partial persistence diagram.

Table 1 aggregates the running times of our implementation of the two approaches. As expected the persistence running time in the medial axes approach is lower than in the link approach (about 3 times lower). Nevertheless, concerning the filtration(s) construction, the medial axes approach is about 1.5 slower than the link approach due to our current implementation. There is room for optimization in the filtration(s) construction step, which is currently much slower than the persistence step using PHAT.

6. Conclusion

We developed new methods to compute measures of holes in volumetric shapes. In addition we implemented it for 3D objects represented by a surface mesh. Our approach is based on the theory of persistent homology and uses the notion of medial axis, which provides a powerful link between geometry and topology. Both of our methods intend to compute every hole-ball of the analyzed shape, and one of both also provides the pairing between thickness-balls and breadth-balls. An advantage of our approach is that it directly focuses on the part that carries the information we need: the medial axis. From a complexity point of view, this is an important advance because the computation of hole measures does not require an expensive triangulation of the space but

3D model	sampling size	Medial axes approach			Link approach			Number of holes
		total size of the filtrations	filtration time (s)	persistence time (s)	size of the filtration	filtration time (s)	persistence time (s)	
gear	11 182	261 406	24.92	2.94	321 825	16.81	10.40	13
four-components	6 536	145 166	12.47	1.70	181 405	8.35	5.69	7
hollow-cubic-ball	5 434	108 674	9.74	1.57	126 513	6.83	4.19	6
triakis-tetrahedron	3 745	81 178	6.42	1.32	100 751	4.16	3.05	12
knot	3 200	74 896	6.02	1.19	91 325	4.13	2.83	2
egg-in-a-box	1 727	27 184	2.63	0.70	32 011	1.62	1.01	3
two-rings	1 000	22 564	1.54	0.64	26 473	1.08	1.02	4
eight	315	7 396	0.51	0.29	8 699	0.33	0.42	3
two-cubes	196	2 300	0.25	0.11	2 541	0.20	0.25	2

Table 1: Summary of the experiments, comparing sampling size (points per model), filtration size (total number of elements in the inner and outer medial filtrations combined and number of elements in the Voronoi filtration), running time for the construction of the filtration(s) and running time for the persistent homology algorithm.

simply a discretization of the mesh surface and computation of the persistence on the medial axes.

From a theoretical point of view, we extended the definition of hole measure to arbitrary volumetric objects and put forward the theoretical links between geometry and topology that are provided by medial axes and persistent homology. Yet, to fully ensure the correctness of our methods, some conjectures about algebraic topology and discrete geometry still remain to be proved (see Conjectures 4.1, 4.7 and 5.1).

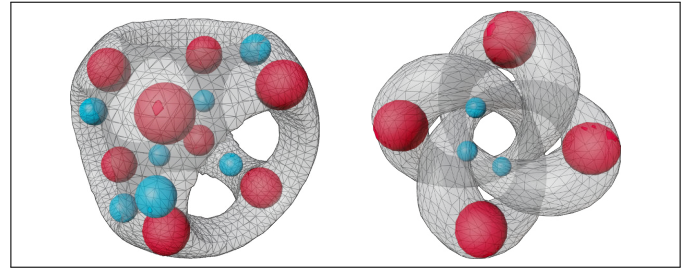
Future work and prospects. As highlighted in Section 5.3, the major stake of our approach is about the sampling. A future work would be to implement an ϵ -sampling algorithm. Such an algorithm is provided in [23]. It essentially needs to compute a local lower bound of the distance to the medial axis. However, this lower bound is often obtained by computing the medial axis, which is what we want to compute with the ϵ -sampling.

A solution to this vicious circle would be to first use a sufficiently precise uniform sampling in order to compute this lower bound, then compute an ϵ -sampling and finally use the resulting set to approximate the medial axis. Another idea is to first run the whole algorithm on the first sampling, and refine near the sample points that induced hole measures.

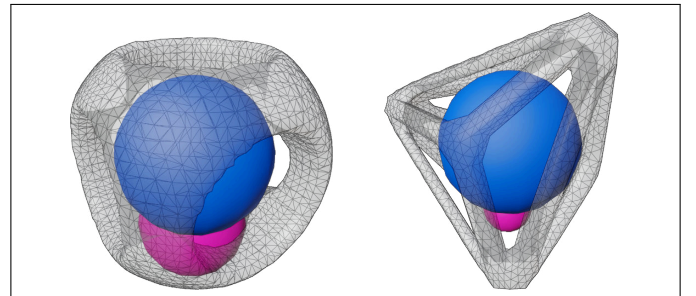
An additional implementation improvement would be to use a more appropriate medial axis approximation. A good candidate is the *core* [9] because it is smaller than the medial axis and preserves homology and topologically critical points. However, it also needs an ϵ -sampling. Additionally, it uses the notion of *unstable flow complex*, which is numerically unstable and must be implemented with exact computation (see [15]).

We plan to compute the hole measures on the CAD models of the ABC dataset [24] and compare them to the geometrical parameters of their holes. Intuitively, the hole measure should coincide with those values. This could be used as a formal topological method in CAD reverse engineering.

Another relevant geometric hole descriptor is the notion of *minimal cycles*. Minimal cycles are homology generators that minimize a quantity (typically a length, area or volume depending on the dimension of the cycle). The extended notion of *minimal persistent cycles* was introduced in [25]: minimal persistent cycles correspond to minimal cycles along a filtration and can be associated to points in a persistent diagram. We plan to put in parallel this concept with our hole balls, as they both represent two different geometrical measures of topological holes.



(a) hole-balls of 0-holes (including non-present holes) for *hollow-cubic-ball* and *knot*. Light blue balls are B -balls with $B < 0$.



(b) hole-balls of non-present 2-holes for *hollow-cubic-ball* and *triakis-tetrahedron*. Magenta balls are T -balls with $T < 0$.

Figure 14: hole-balls of non present holes.

Lastly, both our methods compute not only the present holes but also every late-birth and early-death holes. It is possible to extend the definition of hole-balls for those non-present holes, potentially inducing negative thickness or breadth. Even though those holes are not present in the object, their hole-balls can give interesting intuitive geometrical information. For instance, non-present holes of dimension 0 can give a hint about how to segment an object in a meaningful way (see Fig. 14(a)). Non-present holes of dimension 2 can tell where the object looks like a cage or a prison and where is the easiest place for a ball to escape it (see Fig. 14(b)). It may be interesting to investigate this idea a bit further.

References

- [1] F. Chazal, D. Cohen-Steiner, L. Guibas, F. Méholi, S. Oudot, Gromov-Hausdorff stable signatures for shapes using persistence, *Comput. Graph. Forum* 28 (2009) 1393–1403. doi:10.1111/j.1467-8659.2009.01516.x.
- [2] A. Gonzalez-Lorenzo, A. Bac, J.-L. Mari, P. Real, Two Measures for the Homology Groups of Binary Volumes, in: Springer (Ed.), 19th IAPR International Conference on Discrete Geometry for Computer Imagery (DGCI 2016), Vol. 9647 of Discrete Geometry for Computer Imagery, Nantes, France, 2016, pp. 154–165. doi:10.1007/978-3-319-32360-2_12. URL <https://hal-amu.archives-ouvertes.fr/hal-01341015>
- [3] A. Hatcher, C. U. Press, C. U. D. of Mathematics, Algebraic Topology, Algebraic Topology, Cambridge University Press, 2002. URL <https://books.google.fr/books?id=BjKs86kosqgC>
- [4] H. Edelsbrunner, J. Harer, Persistent homology—a survey, *Discrete and Computational Geometry - DCG 453*. doi:10.1090/conm/453/08802.
- [5] P. Alexandroff, Über die metrisation der im kleinen kompakten topologischen räume, *Mathematische Annalen* 92 (1924) 294–301.
- [6] A. Tagliasacchi, T. Delame, M. Spagnuolo, N. Amenta, A. Telea, 3D skeletons: A state-of-the-art report, *Computer Graphics Forum* 35. doi:10.1111/cgf.12865.
- [7] T. Culver, J. Keyser, D. Manocha, Exact computation of the medial axis of a polyhedron, *Comput. Aided Geom. Des.* 21 (1) (2004) 65–98. doi:10.1016/j.cagd.2003.07.008. URL <https://doi.org/10.1016/j.cagd.2003.07.008>
- [8] N. Amenta, S. Choi, R. Kolluri, The power crust, unions of balls, and the medial axis transform, *Computational Geometry* 19. doi:10.1016/S0925-7721(01)00017-7.
- [9] J. Giesen, E. Ramos, S. Bardia, Medial axis approximation and unstable flow complex, *International Journal of Computational Geometry and Applications* 18. doi:10.1142/S0218195908002751.
- [10] T. K. Dey, W. Zhao, Approximate medial axis as a Voronoi subcomplex, *Computer-Aided Design* 36 (2) (2004) 195–202, solid Modeling and Applications. doi:https://doi.org/10.1016/S0010-4485(03)00061-7. URL <https://www.sciencedirect.com/science/article/pii/S0010448503000617>
- [11] A. Lieutier, Any open bounded subset of \mathbb{R}^n has the same homotopy type than its medial axis, in: Proceedings of the Eighth ACM Symposium on Solid Modeling and Applications, SM '03, Association for Computing Machinery, New York, NY, USA, 2003, p. 65–75. doi:10.1145/781606.781620. URL <https://doi.org/10.1145/781606.781620>
- [12] F. Chazal, R. Soufflet, Stability and finiteness properties of medial axis and skeleton, *Journal of Dynamical and Control Systems* 10 (2004) 149–170. doi:10.1023/B:JODS.0000024119.38784.ff.
- [13] R. Hardt, Triangulation of subanalytic sets and proper light subanalytic maps, *Inventiones Mathematicae* 38 (1976) 207–217. doi:10.1007/BF01403128.
- [14] F. Chazal, A. Lieutier, The λ -medial axis, *Graphical Models graphical Models and Image Processing computer Vision, Graphics, and Image Processing* 67 (2005) 304–331.
- [15] F. Cazals, A. Parameswaran, S. Pion, Robust construction of the three-dimensional flow complex, in: ACM Symposium on Computational Geometry (SCG), Washington, United States, 2008, pp. 182–191. URL <https://hal.inria.fr/inria-00344962>
- [16] D. Siersma, Voronoi diagrams and Morse theory of the distance function.
- [17] C. Jamin, S. Pion, M. Teillaud, 3D triangulations, in: CGAL User and Reference Manual, 5.2.2 Edition, CGAL Editorial Board, 2021. URL <https://doc.cgal.org/5.2.2/Manual/packages.html#PkgTriangulation3>
- [18] U. Bauer, M. Kerber, J. Reininghaus, H. Wagner, PHAT – persistent homology algorithms toolbox, in: H. Hong, C. Yap (Eds.), *Mathematical Software – ICMS 2014*, Springer Berlin Heidelberg, Berlin, Heidelberg, 2014, pp. 137–143.
- [19] Q. Zhou, A. Jacobson, Thingi10K: A dataset of 10,000 3D-printing models, arXiv preprint arXiv:1605.04797.
- [20] Y.-S. Gazull, A. Gonzalez-Lorenzo, A. Bac, Computing Geometrical Measures of Topological Holes, <https://github.com/Yann-Situ/Hole-Measures/releases/tag/paper-submission> (2023).
- [21] N. Amenta, D. Attali, O. Devillers, Complexity of Delaunay triangulation for points on lower-dimensional polyhedra, in: Proceedings of the Eighteenth Annual ACM-SIAM Symposium on Discrete Algorithms, SODA '07, Society for Industrial and Applied Mathematics, USA, 2007, p. 1106–1113.
- [22] R. Dwyer, Higher-dimensional Voronoi diagrams in linear expected time., *Discrete and computational geometry* 6 (4) (1991) 343–368. URL <http://eudml.org/doc/131163>
- [23] J.-D. Boissonnat, S. Oudot, Provably good sampling and meshing of surfaces, *Graphical Models* 67 (5) (2005) 405–451, solid Modeling and Applications. doi:https://doi.org/10.1016/j.gmod.2005.01.004. URL <https://www.sciencedirect.com/science/article/pii/S1524070305000056>
- [24] S. Koch, A. Matveev, Z. Jiang, F. Williams, A. Artemov, E. Burnaev, M. Alexa, D. Zorin, D. Panozzo, ABC: A big CAD model dataset for geometric deep learning, in: The IEEE Conference on Computer Vision and Pattern Recognition (CVPR), 2019.
- [25] T. K. Dey, T. Hou, S. Mandal, Computing minimal persistent cycles: Polynomial and hard cases, CoRR abs/1907.04889. arXiv:1907.04889. URL <http://arxiv.org/abs/1907.04889>

Appendix A: technical proofs

Homology of inner and outer medial axes

In this section, we explain the complete proof of the following theorem in details:

Theorem 3.3 (Medial axes homology). *Let X be a regular object of \mathbb{R}_*^n , then*

$$\hat{\mathcal{M}}_*(X) \cong X^c \quad \check{\mathcal{M}}_*(X) \cong \check{X}$$

Given Y a nonempty closed subset of \mathbb{R}_*^n whose boundary ∂Y is bounded in \mathbb{R}^n , we define the following function:

$$p_Y : \hat{\mathcal{M}}_*(Y)^c \longrightarrow Y$$

$$y \longmapsto \underset{x \in Y}{\operatorname{argmin}}(d(x, y))$$

Lemma 6.0.1. *p_Y is well defined and continuous.*

Proof. p_Y is well defined. Indeed:

- if $y \in Y$: we simply have $p_Y(y) = y$.
- If $y \in \hat{\mathcal{M}}_*(Y)^c \setminus Y$: then $y \notin Y$ so we have $d(y, Y) = d(y, \partial Y)$ by closeness of Y . Moreover $y \in \mathcal{M}_*(Y)^c$ (because $\mathcal{M}_*(Y) = \hat{\mathcal{M}}_*(Y) \sqcup \check{\mathcal{M}}_*(Y)$ and $\check{\mathcal{M}}_*(Y) \subset Y$) so $A_Y(y)$ has only one element which is $p_Y(y)$.

Now we prove p_Y is continuous. Firstly, remind that distance functions are continuous. Take $y \in \hat{\mathcal{M}}_*(Y)^c$ and (y_n) a sequence of $\hat{\mathcal{M}}_*(Y)^c$ such that $y_n \xrightarrow{n \rightarrow \infty} y$.

By continuity of distance we have :

$$d(y_n, Y) \xrightarrow{n \rightarrow \infty} d(y, Y)$$

As we consider the sequence $(p_Y(y_n))_{n \in \mathbb{N}}$ in the compact space \mathbb{R}_*^n , Bolzano-Weierstrass theorem implies $\operatorname{Adh}((p_Y(y_n))) \neq \emptyset$. Let's prove that $\operatorname{Adh}((p_Y(y_n))) = \{p_Y(y)\}$:

Let $x \in \operatorname{Adh}((p_Y(y_n)))$. There exists some subsequence i_n such that $(y_{i_n}, p_Y(y_{i_n})) \xrightarrow{n \rightarrow \infty} (y, x)$ so by continuity of distance:

$$d(y_{i_n}, p_Y(y_{i_n})) \xrightarrow{n \rightarrow \infty} d(y, x)$$

As $d(y_{i_n}, Y) \xrightarrow{n \rightarrow \infty} d(y, Y)$ and $d(y_{i_n}, Y) = d(y_{i_n}, p_Y(y_{i_n}))$, we have $d(y, x) = d(y, Y)$. Moreover $x \in Y$ (by closeness of Y).

Hence, by well-definition on p_Y , $x = p_Y(y)$ and $\operatorname{Adh}((p_Y(y_n))) = \{p_Y(y)\}$.

As a result, $p_Y(y_n) \xrightarrow{n \rightarrow \infty} p_Y(y)$ therefore p_Y is continuous. \square

Proof of Theorem 3.3. Let's X be a regular object. We can define the following homotopy:

$$H : [0, 1] \times \hat{\mathcal{M}}_*(X)^c \longrightarrow \hat{\mathcal{M}}_*(X)^c \\ (t, y) \longmapsto tp_X(y) + (1-t)y$$

- H is well defined: Firstly, p_X is well defined. Indeed, by Definition 3.1-1, X is a nonempty closed subset whose boundary is bounded in \mathbb{R}^n .

Secondly, for every t and y we have $H(t, y) \in \hat{\mathcal{M}}_*(X)^c$. To prove that, let y be an element of $\hat{\mathcal{M}}_*(X)^c$. Firstly, $\hat{\mathcal{M}}_*(X) \cap X = \emptyset$ so $p_X(y) \notin \hat{\mathcal{M}}_*(X)$. Let $t \in]0, 1[$ and let $y_t := H(t, y)$. For every $x \in \mathbb{R}^n$ we denote $B(x)$ the minimal closed ball centered in x and intersecting ∂X . In particular, $B(x) \cap \partial X = A_X(x)$.

If $y \in X$ then $y_t \notin \hat{\mathcal{M}}_*(X)$ so we consider the case where $y \notin X$. As y, y_t and $p_X(y)$ are aligned, we have that $B(y_t) \subset B(y)$, in particular, as $A_X(y) = \{p_X(y)\}$ and $A_X(y_t) \neq \emptyset$, we can deduced that $B(y_t) \cap \partial X = \{p_X(y)\}$. This implies that $y_t \notin \mathcal{M}_*(X)$.

- H verifies the properties of a deformation retract from $\hat{\mathcal{M}}_*(X)^c$ to X :

- $X \subset \hat{\mathcal{M}}_*(X)^c$
- $H(0, y) = y$
- $H(1, y) = p_X(y) \in X$
- $\forall t \forall y \in X, H(t, y) = y$
- H is continuous (by Lemma 6.0.1).

As a consequence $\hat{\mathcal{M}}_*(X)^c \cong X$. This directly implies:

$$\hat{\mathcal{M}}_*(X)^c \cong X \quad (1)$$

To conclude the proof, we want to use Alexander duality to “apply” the complementary operator on Eq. 1. To do that, we need to show that the medial axes verifies the necessary properties for Proposition 2.2.

- X is a compact subanalytic subset of \mathbb{R}_*^n , so by Theorem 3.2-2. it is a locally contractible nonempty compact with finitely generated homology groups.
- Similarly, we can deduce from Theorem 3.2 that $\hat{\mathcal{M}}_*(X)$ is a locally contractible set of \mathbb{R}_*^n with finitely generated homology groups. In addition, it is compact because as an intersection of closed sets in \mathbb{R}_*^n : $\check{\mathcal{M}}_*(X) = \mathcal{M}_*(X) \cap X$.

Hence, using Proposition 2.2 on X and $\hat{\mathcal{M}}_*(X)$ we obtain that for all q , $H_q(X^c) \approx H_{n-q-1}(X)$ and $H_q(\hat{\mathcal{M}}_*(X)^c) \approx H_{n-q-1}(\hat{\mathcal{M}}_*(X))$. Therefore the homologous Equation 1 translates to:

$$\hat{\mathcal{M}}_*(X) \cong X^c$$

As $\overline{X^c}$ is also a regular object. Indeed, if p_∞ is in the interior of X , then $X^c = \mathbb{R}^n \setminus X$ is subanalytic (Theorem 3.2-1). If p_∞ is in the interior of X^c , then $X^c = \{p_\infty\} \cup \mathbb{R}^n \setminus X$ is still subanalytic. p_∞ can't be in ∂X because ∂X is bounded in \mathbb{R}^n . Therefore, using Theorem 3.2-1 again, $\overline{X^c}$ is subanalytic. Moreover, it is a regular object because $\partial X = \partial \overline{X^c}$ is nonempty bounded in \mathbb{R}^n .

Applying the whole proof on $\overline{X^c}$ gives:

$$\check{\mathcal{M}}_*(X) \cong \check{X}$$

□

The t -medial axis is the medial axis of the t -erosion

In this section, we explain the complete proof of the following theorem in details:

Theorem 4.2. Given X a regular object and a filtration value $t < 0$:

$$\check{\mathcal{M}}_*(\mathcal{F}_t(X)) = \check{\mathcal{M}}_t(X)$$

Let $t < 0$ (case $t = 0$ of 4.2 is trivial). For simplicity we will write \mathcal{F}_t instead of $\mathcal{F}_t(X)$ The proof of Theorem 4.2 requires the two following lemmas:

Lemma 6.0.2.

$$\partial \mathcal{F}_t \subset sdf_X^{-1}(\{t\})$$

Proof of Lemma 6.0.2. \mathcal{F}_t is open because sdf is continue and p_∞ is in not in ∂X (∂X is bounded in \mathbb{R}^n). Moreover the complementary of $sdf^{-1}([-\infty, t])$ in \mathbb{R}_*^n is $sdf^{-1}([t, +\infty])$.

By definition, the boundary of an open T is $\partial T = \overline{T} \cap T^c$, where \overline{T} is the closure of T and T^c its complementary. Hence, the boundary of \mathcal{F}_t is:

$$\partial \mathcal{F}_t = \overline{sdf^{-1}([-\infty, t])} \cap sdf^{-1}([t, +\infty])$$

By continuity of sdf , the sdf value of a point in $\overline{sdf^{-1}([-\infty, t])}$ is in $[-\infty, t]$.

Therefore, the sdf value of a point in $\partial \mathcal{F}_t$ is in $[-\infty, t] \cap [t, +\infty] = \{t\}$. □

Lemma 6.0.3.

$$\forall c \in \mathcal{F}_t, \quad d(c, \partial X) = d(c, \partial \mathcal{F}_t) - t$$

Proof of Lemma 6.0.3. let us take c in \mathcal{F}_t .

- We choose $x \in A_{\mathcal{F}_t}(c)$ and $\hat{x} \in A_X(x)$. We have the following inequality by triangle inequality:

$$d(c, \partial X) \leq d(c, \hat{x}) \\ \leq d(c, x) + d(x, \hat{x}) \\ \leq d(c, \mathcal{F}_t) + d(x, \partial X)$$

By using the definition of $A_{\mathcal{F}_t}(c)$ and $A_X(x)$.

$x \in \partial \mathcal{F}_t$ so $d(x, \partial X) = -t$ by Lemma 6.0.2. This implies:

$$d(c, \partial X) \leq d(c, \mathcal{F}_t) - t \quad (2)$$

- Conversely, by contradiction, suppose

$$d(c, \partial X) < d(c, \partial \mathcal{F}_t) - t \quad (3)$$

Then let $\hat{x} \in A_X(c)$. As $d(c, \partial X) > -t > 0$, we define:

$$\lambda := \frac{d(c, \partial X) - d(c, \partial \mathcal{F}_t) - t}{2d(c, \partial X)} \\ x := \lambda c + (1 - \lambda)\hat{x}$$

Thus, we have:

$$d(c, x) = (1 - \lambda)d(c, \hat{x}) = \frac{d(c, \partial X) + d(c, \partial \mathcal{F}_t) + t}{2} \\ d(c, x) < d(c, \partial \mathcal{F}_t) \quad \text{using 3.}$$

So, as c is in \mathcal{F}_t , we have $x \in \mathcal{F}_t$.

Moreover we have:

$$d(x, \hat{x}) = \lambda d(c, \hat{x}) = \frac{d(c, \partial X) - d(c, \partial \mathcal{F}_t) - t}{2}$$

$$d(x, \hat{x}) < -t \quad \text{using 3.}$$

So $d(x, \partial X) \leq d(x, \hat{x}) < -t$, therefore we have $x \notin \mathcal{F}_t$. By contradiction we have $d(c, \partial X) \geq d(c, \partial \mathcal{F}_t) - t$.

Thus, with 2 we get:

$$d(c, \partial X) = d(c, \partial \mathcal{F}_t) - t$$

□

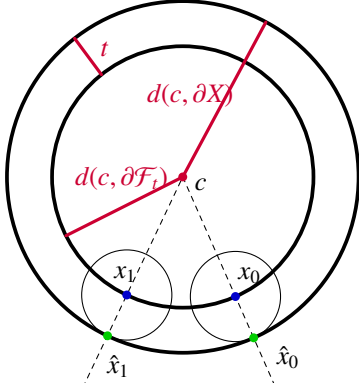


Figure 15: Illustration of the different points defined in the proof of the Theorem 4.2 and Lemma 6.0.3.

Proof of Theorem 4.2.

• **Proof of $\check{\mathcal{M}}_t(X) \subset \check{\mathcal{M}}(\mathcal{F}_t)$:**

let $c \in \check{\mathcal{M}}_t(X)$. We have directly $c \in \check{\mathcal{M}}(X)$ so we choose $\hat{x}_0, \hat{x}_1 \in A_X(c)$ such that $\hat{x}_0 \neq \hat{x}_1$.

As $d(c, \partial X) > -t > 0$, we define:

$$x_0 = \mu c + (1 - \mu)\hat{x}_0$$

$$x_1 = \mu c + (1 - \mu)\hat{x}_1$$

$$\text{with } \mu = \frac{-t}{d(c, \partial X)} \in]0, 1[$$

We easily have $x_0 \neq x_1$.

To prove $c \in \check{\mathcal{M}}(\mathcal{F}_t)$, let us show that x_0 and x_1 belong to $A_{\mathcal{F}_t}(c)$.

Let $i \in \{0, 1\}$. We only need to show $d(x_i, c) = d(c, \partial \mathcal{F}_t)$ and $x_i \in \partial \mathcal{F}_t$:

$$d(x_i, c) = (1 - \mu)d(c, \hat{x}_i)$$

$$= \frac{d(c, \partial X) + t}{d(c, \partial X)} d(c, \partial X)$$

$$= d(c, \partial X) + t \quad \text{by Lemma 6.0.3}$$

Moreover, we have:

$$d(x_i, \hat{x}_i) = \mu d(c, \hat{x}_i) = -t$$

So, as $\hat{x}_i \in \partial X$ we obtain $d(x_i, \partial X) \leq d(x_i, \hat{x}_i) \leq -t$. This implies $x_i \notin \mathcal{F}_t$. x_i is not in \mathcal{F}_t but $d(x_i, c) = d(c, \partial \mathcal{F}_t)$ (with $c \in \mathcal{F}_t$), therefore x_i belongs to $\partial \mathcal{F}_t$.

• **Proof of $\check{\mathcal{M}}(\mathcal{F}_t) \subset \check{\mathcal{M}}_t(X)$:**

let $c \in \check{\mathcal{M}}(\mathcal{F}_t)$. We choose $x_0, x_1 \in A_{\mathcal{F}_t}(c)$ such that $x_0 \neq x_1$.

Let $i \in \{0, 1\}$. Let $\hat{x}_i \in A_X(x_i)$. $x_i \in \partial \mathcal{F}_t$ so by Lemma 6.0.2 we have $d(\hat{x}_i, x_i) = -t$. By triangle inequality we have:

$$d(\hat{x}_i, c) \leq d(\hat{x}_i, x_i) + d(x_i, c) \tag{4}$$

$$\leq -t + d(c, \partial \mathcal{F}_t)$$

$$\leq d(c, \partial X) \quad \text{by Lemma 6.0.3}$$

As \hat{x}_i is in ∂X we obtain $d(c, \partial X) = d(\hat{x}_i, c)$ so \hat{x}_i belongs to $A_X(c)$. To conclude the proof, let us show that $\hat{x}_0 \neq \hat{x}_1$: the triangle inequality 4 is in the equal case, which means that \hat{x}_i, x_i and c are co-linear. As $d(c, \partial X) > -t > 0$, we get:

$$x_0 = \mu c + (1 - \mu)\hat{x}_0$$

$$x_1 = \mu c + (1 - \mu)\hat{x}_1$$

$$\text{with } \mu = \frac{-t}{d(c, \partial X)} \in]0, 1[$$

Hence we have $\hat{x}_0 \neq \hat{x}_1$ since $x_0 \neq x_1$.

□